Impact of the major SSWs of February 2018 and January 2019 on the middle atmospheric nitric oxide abundance

Journal of Atmospheric and Solar–Terrestrial Physics 218 (2021) 105586

Contents lists available at ScienceDirect

Journal of Atmospheric and Solar–Terrestrial Physics

journal homepage: www.elsevier.com/locate/jastp

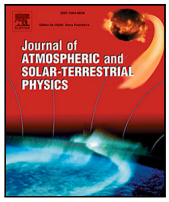

Research paper

Impact of the major SSWs of February 2018 and January 2019 on the middle atmospheric nitric oxide abundance

Kristell Pérot [a,*], Yvan J. Orsolini [b,c]

[a] Chalmers University of Technology, Department of Space, Earth and Environment, SE-412 96 Gothenburg, Sweden
[b] Norwegian Institute for Air Research (NILU), Instituttveien 18, N-2027, Kjeller, Norway
[c] Norwegian University of Science and Technology (NTNU), Trondheim, Norway

ARTICLE INFO

Keywords:
Nitric oxide
Sudden stratospheric warming
Energetic particle precipitation
Middle atmospheric circulation

ABSTRACT

The Arctic middle atmosphere was affected by major sudden stratospheric warmings (SSW) in February 2018 and January 2019, respectively. In this article, we report for the first time the impact of these two events on the middle atmospheric nitric oxide (NO) abundance. The study is based on measurements obtained during two dedicated observation campaigns, using the Sub-Millimetre Radiometer (SMR) aboard the Odin satellite, measuring NO globally since 2003. The SSW of February 2018 was similar to other, more dynamically quiet, Arctic winters in term of NO downward transport from the upper mesosphere–lower thermosphere to lower altitudes (referred to as energetic particle precipitation indirect effect EPP-IE). On the contrary, the event of January 2019 led to one of the strongest EPP-IE cases observed within the Odin operational period. Important positive NO anomalies were indeed observed in the lower mesosphere–upper stratosphere during the three months following the SSW onset, corresponding to NO volume mixing ratios more than 50 times higher than the climatological values. These different consequences on the middle atmospheric composition are explained by very different dynamical characteristics of these two SSW events.

1. Introduction

Nitric oxide (NO) has long been recognised as one of the most important trace gases in the middle and upper atmosphere, due to its role in cooling the thermosphere through mid-infrared emission (Kockarts, 1980; Mlynczak et al., 2003), as an indicator of energy input (e.g. Sinnhuber et al., 2012; Mlynczak et al., 2015), and in its involvement in the ozone catalytic destruction (Crutzen, 1970).

NO chemistry in the mesosphere and lower thermosphere (MLT) consists in a complex scheme of coupled reactions, strongly influenced by solar and geomagnetic activity (Brasseur and Solomon, 2005). Solar irradiance and energetic particle precipitation (EPP) are the main sources of ionisation and dissociation in this region, and provide the necessary elements for NO chemistry to take place (Barth and Bailey, 2004; Sinnhuber et al., 2012). EPP refers to the process by which energetic charged particles, protons and electrons, precipitate into the Earth's atmosphere and affect the chemistry through neutral and ionic reactions. These particles originate either directly from the Sun in case of solar proton events or else from the Earth's magnetosphere and radiation belts. The latter are electrons which precipitate into the polar atmosphere along magnetic field lines during auroras or geomagnetic perturbations arising from the interaction between the solar wind and the magnetosphere. The altitude range over which a particle penetrates into the atmosphere is determined by its energy. The most energetic of these electrons (called medium energy electrons, MEE) can penetrate into the lower mesosphere, e.g. during geomagnetic storms, while lesser energetic auroral electrons do not penetrate deeper than the mesopause region (Mironova et al., 2015). In the MLT, the NO vertical distribution is characterised by a strong increase in concentration with height, reaching a maximum around 110 km (Siskind et al., 1998). Previous studies have shown that, in this atmospheric region, the precipitation of auroral electrons is the main source of NO at high latitudes, while solar soft X-rays have a more important contribution at lower latitudes (e.g. Kiviranta et al., 2018).

Under sunlit conditions, in the MLT, NO has a chemical lifetime of less than one day, whereas it may persist for several weeks during polar winter due to the absence of sunlight. Through diffusion and eddy mixing and, occasionally, through large-scale downward advection, NO can thus be transported from its MLT reservoir into the upper mesosphere. In particular, the downward branch of the middle atmospheric residual circulation brings the NO-enriched air masses to lower mesospheric and stratospheric altitudes. This thermospheric and mesospheric production by EPP followed by winter-time downward

* Corresponding author.
E-mail address: kristell.perot@chalmers.se (K. Pérot).

https://doi.org/10.1016/j.jastp.2021.105586
Received 13 November 2020; Received in revised form 3 February 2021; Accepted 5 February 2021
Available online 20 March 2021

transport of NO into the stratosphere at high latitudes is generally referred to as the EPP indirect effect (EPP-IE; Randall et al., 2007). There is a distinct inter-annual variability of this descent in the northern hemisphere however, as a strong NO descent occurs during particularly major sudden stratospheric warming (SSW) events associated with an elevated stratopause (hereafter, ES-SSWs) (Manney et al., 2009; Pérot et al., 2014; Orsolini et al., 2017). Following the onset of ES-SSWs, there is a marked jump in the altitude of the stratopause that reforms at altitudes corresponding normally to mesospheric heights. During such events, planetary waves generated in-situ in the middle atmosphere provide a strong forcing of the zonal-mean flow and are – for a brief period following the onset – the main driver of a strong downward meridional residual circulation near the mesopause. This reversal of the lower thermospheric residual circulation (climatologically upwards in winter, overlying the downwards meridional residual circulation below) (Lossow et al., 2009; Limpasuvan et al., 2016; Orsolini et al., 2017) can bring down more NO from the MLT reservoir into the mesosphere. Not all SSWs are accompanied by an elevated stratopause however (Chandran et al., 2013), as will be illustrated below.

Once in the stratosphere, the NO_x chemical family ($NO + NO_2$) plays a crucial role, because it is involved in the main catalytic cycle responsible for ozone (O_3) depletion between about 25 and 40 km (Crutzen, 1970). Based on ten years of satellite observations, Funke et al. (2014) showed that NO_x produced by EPP (hereafter, EPP-NO_x), together with other chemically associated reactive nitrogen species (NO_y) reaches down to altitudes below 30 km in both hemispheres in almost all the winters observed. Resulting changes in O_3 concentrations corresponding to an average depletion of 10%–15% have been documented in satellite observations (e.g. Fytterer et al., 2015; Damiani et al., 2016). Model studies even suggest that ozone loss can continue throughout polar summer after large SSWs (Sinnhuber et al., 2018). In turn, changes in O_3 have the potential to alter the radiative budget, and thus the dynamics, of the middle atmosphere (Sinnhuber et al., 2018; Guttu et al., 2020). Several studies based on comparisons of NO between state-of-the-art chemistry climate models and satellite observations have highlighted that, despite some recent improvements, the amount of EPP-NO transported down is still significantly underestimated in the models, especially after major SSWs (e.g. Funke et al., 2017; Orsolini et al., 2017). This deficiency makes it difficult to quantify the effect of EPP on O_3 and middle atmosphere dynamics in models, with potential implications for climate modelling. EPP is a potential contributor to the solar influence on climate, and has been recommended for the first time as a solar forcing parameter for the CMIP-6 model studies (Matthes et al., 2017). To this end, it is capital to provide high-quality satellite observations of NO to benchmark new model simulations.

Currently, the Sub-Millimetre Radiometer (SMR) aboard the Odin satellite is the only instrument that provides global coverage of middle atmospheric NO. We present in this paper the evolution of NO concentration during two remarkable SSW events in the recent winters 2017–2018 and 2018–2019, based on dedicated measurement campaigns, and put it in perspective using the unique long-term record of Odin/SMR NO observations since 2003.

2. Data sets

2.1. Odin/SMR

Odin is a Swedish-led research satellite mission, launched in 2001 in cooperation with the Canadian, French and Finnish space agencies (Murtagh et al., 2002). It became an European Space Agency (ESA) third party mission in 2007. The satellite is orbiting the Earth in a sun-synchronous orbit at an initial altitude of 580 km and a 18:00 local time ascending node. These parameters are slightly varying with time due to the drifting orbit. Odin was initially a joint astronomy and aeronomy mission and, before April 2007, the observation time was equally divided between the two disciplines. Since this date, the satellite is entirely dedicated to atmospheric observations. Two instruments are aboard the Odin platform, namely the Sub-Millimetre Radiometer (SMR) and the Optical Spectrograph and InfraRed Imager System (OSIRIS). Our study is based on NO measurements performed by SMR.

The sub-millimetre radiometer is a limb emission sounder measuring globally a variety of trace gases as well as temperature in the middle atmosphere. It uses four sub-millimetre channels (486.1–503.9, 541.0–558.0, 547.0–564.0, 563.0–581.4 GHz) and one millimetre-wave channel (118.25–119.25 GHz) (Merino et al., 2002). The observation of different species requires channel switching. Nitric oxide is retrieved from the observation of two thermal emission lines in a band centred near 551.7 GHz, corresponding to the Odin/SMR frequency mode 21 (FM21). The retrieval is based on an optimal estimation technique and the obtained product consists in volume mixing ratio (vmr) profiles (Eriksson, 2020). NO is measured from 45 to 120 km of altitude, during both day- and nighttime, with a latitudinal coverage between 82.5°S and 82.5°N. SMR is at present the only instrument providing NO observational data on a global scale. Systematic errors amount to 3% from spectroscopic parameters, 2% from calibration and 3%–6% from sideband suppression (Sheese et al., 2013). The vertical resolution is approximately 3–4 km in the upper stratosphere, 7 km in the mesosphere up to 80 km and increases to 10 km in the upper mesosphere–lower thermosphere. NO observational programme started in October 2003 and is still ongoing, making this data set one of the longest NO concentration records available for the middle atmosphere. Bender et al. (2015) showed that the version 2.1 of SMR NO data was consistent with NO measurements from SCIAMACHY (SCanning Imaging Absorption spectroMeter for Atmospheric CHartographY), MIPAS (Michelson Interferometer for Passive Atmospheric Sounding) and ACE-FTS (Atmospheric Chemistry Experiment - Fourier Transform Spectrometer), despite the different measurement methods and retrieval strategies used for these four instruments. The data set has recently undergone a full reprocessing. The version 3.0 of SMR level 2 NO data is used in our study. Although no rigorous validation study has yet been carried out for this latest data version, Kiviranta et al. (2018) showed that an empirical model simulating NO concentration in the MLT, based on SMR v3.0 measurements, could reproduce to a large extent the NO variability observed by several other instruments (namely, SOFIE (Solar Occultation For Ice Experiment), SCIAMACHY, ACE-FTS and MIPAS). This constitutes an indirect comparison between these different data sets, showing that they are in good agreement with each other.

In the beginning of the mission, NO was measured one day per month. As previously said, the instrument has been entirely dedicated to atmospheric observations since 2007. NO measurements could therefore be performed much more frequently after this date, on an irregular basis of two observation days in a 14-day cycle (4 to 5 days per month). This corresponds to the standard observation schedule. Owing to SMR operational flexibility, dedicated observations in a specific frequency mode and/or with specific settings can be relatively easily scheduled. Such dedicated observational campaigns took place during the two northern winters 2017–2018 and 2018–2019, based on the alerts for developing SSW issued by forecasting centres. Hence, we carried out two NO measurement campaigns, from 06-02-2018 to 25-04-2018 and from 26-12-2018 to 25-04-2019, respectively, in order to be able to study more accurately the impact of the dynamical perturbations on the middle atmospheric NO concentrations. During these two periods, the frequency mode 21 was used for five consecutive days in the beginning, in order to cover the onset of the SSW events, and for two consecutive days in a four-day cycle then (with a few observation gap periods, due to instrumental technical problems). This led to up to 4700 NO profiles per month, globally, while the average number of profiles per month is approximately 2000, under normal conditions.

2.2. MERRA-2

In order to look at the dynamical state of the middle atmosphere during the two winters under consideration, we are using wind and temperature data from the Modern-Era Retrospective analysis for Research and Applications version 2 (MERRA-2) (Gelaro et al., 2017). Reanalyses integrate satellite-based data and conventional weather observations into a modelling framework to provide Earth system datasets that are continuous in space and time. MERRA-2 is a global atmospheric reanalysis produced by the National Aeronautics and Space Administration (NASA) using the Goddard Earth Observing System Model version 5 (GOES-5) with its Atmospheric Data Assimilation System (ADAS) version 5.12.4. It has a horizontal resolution of 0.625° × 0.5°, 72 vertical levels going from 985 to 0.01 hPa (from the troposphere to the upper mesosphere) and covers the period 1980-present. In our study, we use the three dimensional 3-hourly time-averaged assimilated meteorological fields (data set name M2T3NVASM) (Global Modeling and Assimilation Office (GMAO), 2015). A detailed description of this product, and of MERRA-2 data in general, can be found in Bosilovich et al. (2016) and Bosilovich et al. (2015).

3. Middle atmospheric dynamics during two recent northern winters

Various criteria exist for determining the occurrence of a major sudden stratospheric warming, but the most commonly used definition relies on the reversal of the zonal-mean zonal wind at a latitude of 60° and at a pressure level of 10 hPa (Charlton and Polvani, 2007). The time of the reversal is hereafter referred to as the central date, or onset of the SSW event. We have therefore started our comparison of the dynamical conditions during the northern winters 2017–2018 and 2018–2019 by looking at the MERRA-2 zonal-mean zonal wind at 60° and 10 hPa, from early October to early May, as shown in Fig. 1. The MERRA-2 climatological mean over the period 1980–2019 is also shown, as well as a measure of the inter-annual variability (expressed as plus and minus one standard deviation) and the minimum and maximum values encountered during this period. This plot shows that the climatological high-latitude circulation is characterised by persistent westerlies throughout the boreal cold season, associated with the polar vortex. The zonal winds climatologically reverse in April, indicating the stratospheric final warming. The evolution of the zonal-mean zonal wind during the winter 2017–18 is represented by the green line. It followed the climatological evolution until early February, when it suddenly reversed on the 11th. The easterlies reached particularly high values (up to −24 m/s), and persisted for several weeks. As we can see in Fig. 1, those actually correspond to the strongest zonal-mean easterlies observed at this latitude and height in late February since 1980. The polar vortex only weakly recovered, with westerlies lying within the climatological range until the stratospheric final warming in mid-April, close to the date of its climatological occurrence. The evolution of the zonal-mean zonal wind during the winter 2018–19 is represented by the purple line. We can see that this winter was also characterised by a major SSW event, with a reversal of the westerlies starting on January 01. The easterlies reached values of about -10 m/s and persisted for almost three weeks. The polar vortex then recovered and the zonal-mean westerlies increased until mid-March when values over 50 m/s were the strongest observed during that time of the year since 1980 at 10 hPa. They then decreased and the final warming occurred in late April. The zonal-mean circulation at high latitudes during these two northern winters is next examined using MERRA-2 over a broader range of altitudes encompassing the stratosphere and the lower mesosphere.

3.1. Winter 2017–2018

The SSW of February 2018 can be characterised as a vortex split event, given the predominance of the wave-2 at the onset. It was nevertheless preceded by a preliminary planetary wave pulse in mid-January, primarily from wave-1 (Lü et al., 2020; Xie et al., 2020). While the pronounced impacts of the SSW in the troposphere in the form of cold air outbreaks over Europe, Asia and North America in February and March have been studied (Karpechko et al., 2018; Lü et al., 2020; Overland et al., 2020; Knight et al., 2020), there have been few studies of the stratosphere–mesosphere coupling during this event. A notable exception is Wang et al. (2019) who observed the mesospheric zonal wind reversal and carbon monoxide (CO) abundance in the layer 70–85 km using ground-based microwave remote sensing at a mid-latitude site. Fig. 2a shows the evolution of the MERRA-2 zonal-mean zonal wind, averaged in the latitude band 70–90°N, as a function of height. Transient zonal-mean easterlies appear in the mesosphere already in December and in late January, but the reversal occurred nearly simultaneously from the lower mesosphere through the mid-stratosphere two weeks later. As we can see in the lower panel, the polar stratopause lowers dramatically by about 20 km around the onset of the event, in agreement with previous studies (Limpasuvan et al., 2016). By approximately one month after the central date, the westerlies have clearly recovered at mesospheric altitudes, while in the stratosphere the recovery is only partial and of short duration with the zonal-mean zonal winds thereafter oscillating between weak easterlies and weak westerlies. While the stratopause displays a weak double structure in early March, with a temperature maximum at 50 km and another weaker maximum about 10 km higher, this event does not reveal a distinct characteristic elevated stratopause, as observed for example during the vortex split events of 2009 or 2013 (Pérot et al., 2014). The polar zonal-mean mesospheric cooling is not very pronounced, with temperatures remaining above 210 K (Fig. 2c). Wang et al. (2019) showed that there is no indication of an elevated secondary maximum in zonal-mean temperature, neither of mesospheric large-scale vertical ascent and cooling, based on CO observations at mid-latitudes (47-52°N) from MLS (Microwave Limb Sounder) and from a ground-based microwave radiometer, and on temperature observations from MLS.

3.2. Winter 2018–2019

The 2018–2019 SSW was a mixed-type event with a pronounced wave-1 displacing the polar vortex prior to the onset while, around the time of the onset, the wave-1 was accompanied by a significant contribution from a wave-3. Prolonged subsequent wave forcings from both wave-1 and wave-2 led to a complex break-up of the polar vortex into several lobes (Rao et al., 2019; Lee and Butler, 2020). While these studies examined stratosphere–troposphere coupling and the event predictability, its impact on the mesosphere has up to now barely been studied, with the exception of Shepherd et al. (2020), who used ground-based optical and radar measurements in the high Arctic as well as MLS observations to characterise the SSW. Shi et al. (2020) also looked at the impact of this event on the mesosphere, but they focused on the mid-latitudes. Fig. 2 shows the evolution of the MERRA-2 zonal-mean zonal wind 2b) and temperature (2d) as a function of height throughout the winter 2018–2019. Albeit the onset occurred on January 01, the figure reveals that the polar cap zonal-mean zonal wind reversed nearly simultaneously throughout the mesosphere on December 24 already. In contrast to the previous year, the SSW of 2019 did not lead to marked surface cooling episodes, perhaps due to counteracting influences from the tropics (Knight et al., 2020). On the other hand, the event exhibited the characteristics of an elevated stratopause event. The strong warming in the upper stratosphere was associated with a pronounced mesospheric cooling, with temperatures below 200 K, as seen in Fig. 2d. In MERRA-2, the stratopause reformed around 70 km, although the re-analyses appear to underestimate the

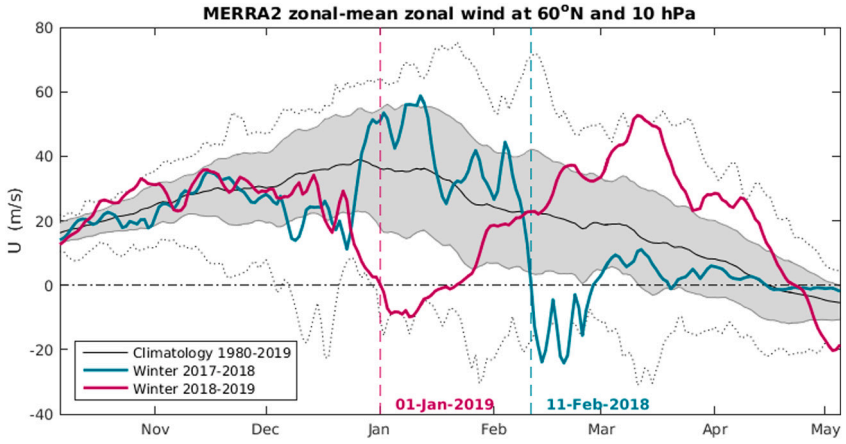

Fig. 1. MERRA-2 zonal mean zonal wind at 60°N and 10 hPa during the winter 2017–18 (in green) and the winter 2018–19 (in purple). The vertical dashed lines indicate the central dates for each of the sudden stratospheric warming events under consideration. The MERRA-2 winter-time zonal wind climatology is also shown. The black line corresponds to the average over the period 1980–2019, the shaded area represents the wind values within one standard deviation of the mean, and the dotted lines show the minimum and maximum values encountered during this period.

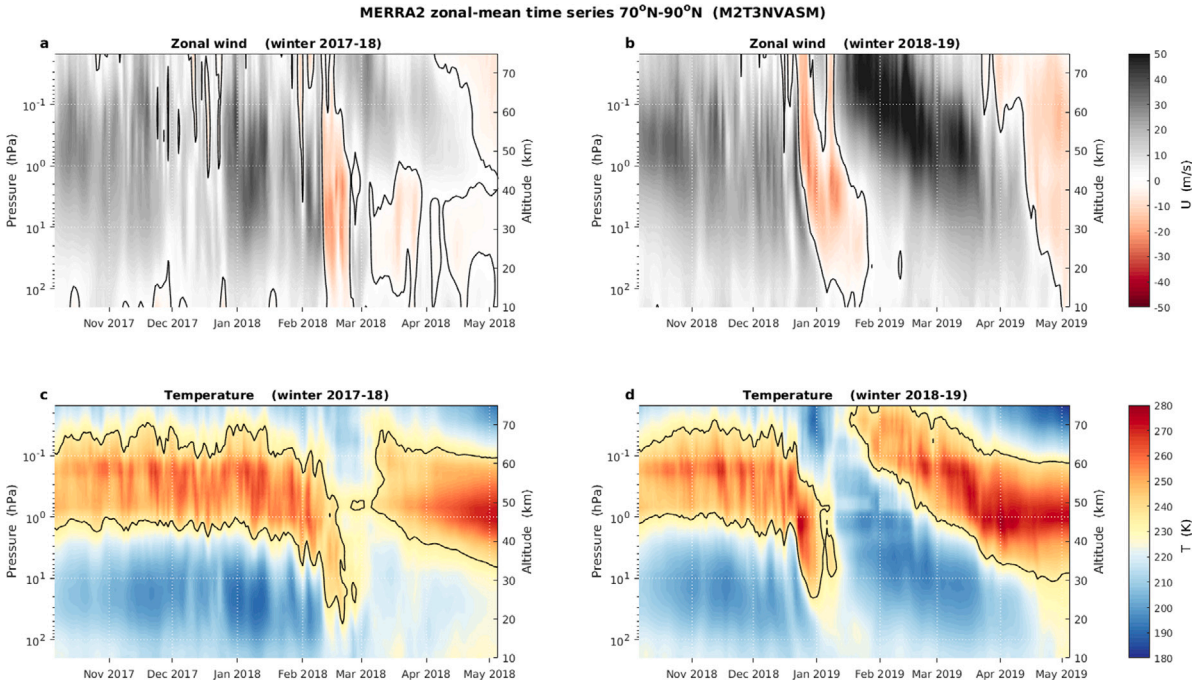

Fig. 2. Winter-time evolution of the MERRA-2 polar cap (70–90°N) zonal mean zonal wind (upper panels) and temperature (lower panels), as a function of altitude, from October to May, for the winters 2017–18 (left panels) and 2018–19 (right panels). The black contour lines correspond to 0 m/s and to 235 K, respectively.

reformation altitude −75 km according to MLS (Shepherd et al., 2020)- due to limitations imposed by the model upper boundary. The strong recovery of the polar vortex previously discussed at 10 hPa is seen to start in the mesosphere already in mid-January (Fig. 2b). Shi et al. (2020) showed, based on MLS carbon monoxide measurements, that the descent motion associated with the recovered vortex extended at significantly lower altitudes in 2019 than in 2018 (compared to the results of Wang et al. (2019).

The comparison between Fig. 2 left and right panels confirms that the January 2019 event has had considerably more impact on the dynamics at mesospheric altitudes than the February 2018 event. Its impact on the composition of the mesosphere has yet been little studied, and the effects of both SSW events on the middle atmospheric NO abundance is described for the first time in the following section.

4. Impact on the NO concentration

The evolution of the NO volume mixing ratios at latitudes greater than 70°N is shown in Fig. 3 (upper panel), as observed by Odin/SMR from October 2003 until April 2019. The black stars on the top of the plot indicate the days when measurements were made. Those highlight the significantly higher temporal sampling starting from 2007, when the astronomy part of the Odin mission ended, as explained in Section 2. In the lower thermosphere, a 11-year cycle signature clearly appears, with higher NO vmr values during the declining phases of solar cycles 23 and 24 (in 2004–2007 and 2015–2018). This is due to a higher geomagnetic activity during these periods, combined with a relatively important solar activity near the solar maximum, leading to an increased production of NO (e.g. Hendrickx et al., 2015). The relative contributions of solar and geomagnetic activities to the

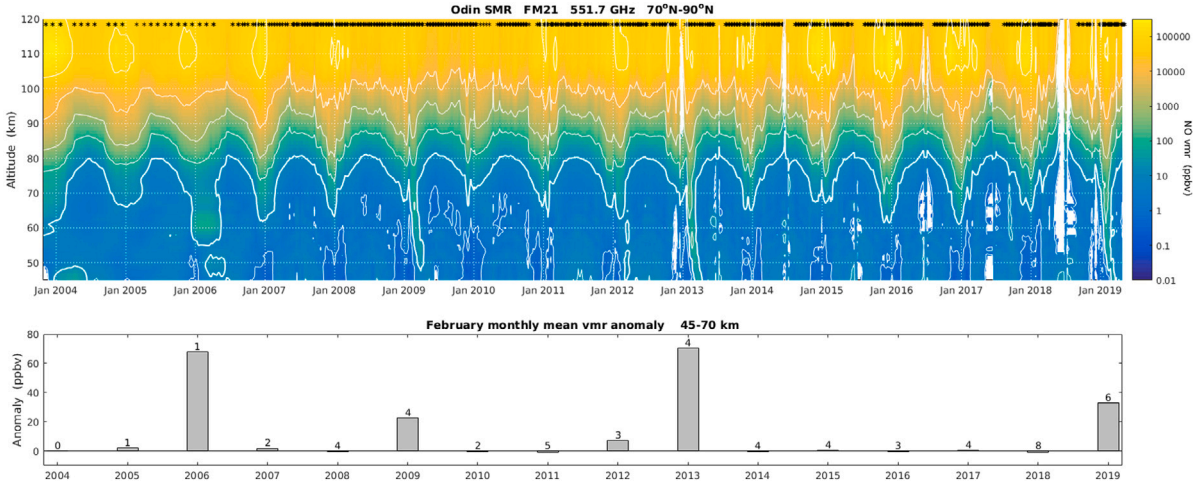

Fig. 3. Upper panel: SMR NO polar cap (70°N-90°N) time series as a function of altitude. The whole operational time period of frequency mode 21 of the Odin satellite, starting in October 2003, is represented. The contour lines correspond to the same levels as those indicated in Fig. 4, but have not been labelled here, for the sake of clarity of the figure. The thicker one corresponds to a volume mixing ratio of 10 ppbv. Black stars on the top of the plot indicate the days when measurements were made. Lower panel: Monthly mean NO vmr anomaly, in the lower mesosphere–upper stratosphere and in the same latitude band, for the month of February. The anomaly is defined as the absolute difference between the measured vmr and the SMR "quiet winter" climatological value on the same day (see Section 4 for more details). The number of FM21 observation days in February is indicated on the top of each bar.

NO variability in this altitude region have been analysed in detail by Kiviranta et al. (2018). Lower down, the NO vmrs display a strong seasonal variability, with higher values in winter, due to the downward transport of NO-enriched air masses from the upper mesosphere–lower thermosphere reservoir to the lower mesosphere –upper stratosphere, as explained in Section 1. This EPP-IE is noticeably stronger in some specific years, namely 2004, 2006, 2009 and 2013. All these winters are characterised by a particularly strong vortex recovery following an ES-SSW event, leading to unusually important NO amounts in the upper stratosphere, as described in previous studies (e.g. Randall et al., 2005, 2006, 2009; Pérot et al., 2014; Orsolini et al., 2017). As it can be seen, the ES-SSW event of 2019 led to one of the strongest descents in the record.

In Fig. 4, we are focusing on the two Arctic winters 2017–18 and 2018–19 described in Section 3, during which two special SMR observation campaigns were carried out (see Section 2), in order to further study the impact of these SSWs on the middle atmospheric composition, and especially on NO abundance. The upper and middle panels represent the temporal evolution of polar cap NO vmr during the two winters under consideration from early October to early May, in the latitude band (70–90°N). In all panels, cross hatch patterns indicate areas with a measurement response (MR) lower than 0.7. The measurement response is defined, for each profile, as the sum of the rows of the averaging kernel matrix (Rodgers, 2000). This constitutes a measure of the relative contribution of the measurement and the a priori to the retrieved profile. All values are represented here, for the sake of completeness, but those with a low MR (between 70 and 85 km when the NO concentration is low, and above 115 km) are influenced by the a priori and should therefore be interpreted with caution. The black stars on the top of the first two panels highlight the fact that NO was measured much more frequently during the dedicated observation campaigns, starting a few days before the central dates of the SSW events (represented by the thick dashed lines) and continuing during the following months (see Section 2 for more details). Although the data gap between mid-November and mid-December 2018 prevents a full overview of the NO reservoir evolution for this second winter, it can be seen that the NO vmr in the lower thermosphere was more important before the SSW event of February 2018 than before the event of January 2019. This can be explained by differences in geomagnetic activity. The mean Kp-index during the three months preceding the SSW central date was indeed slightly higher in 2017–18 than in 2018–19 (1.41 and 1.28, respectively, based on the Kp-index data from the German Research Center for Geosciences, available at https://www.gfz-potsdam.de/en/kp-index/). Despite this difference, a tongue of increased NO concentrations was observed following the 2019 SSW event, with mixing ratios of several tens of ppbv in the lower mesosphere–upper stratosphere, while this was not the case after the 2018 event. In order to put the EPP-IE during these two winters in perspective, we compare it to the NO vmrs usually observed by SMR when the polar vortex is not strongly disturbed by planetary waves, as shown in the lower panel of Fig. 4. This plot represents the Arctic SMR NO vmr as a function of time and altitude, averaged over all the winters with low or moderate dynamical activity (i.e. the winters that were not affected by a reversal of the zonal-mean zonal wind at 60°N and 10 hPa for more than seven consecutive days between November and March), hereafter referred to as "quiet winter" climatology. This evaluation was made based on MERRA-2 zonal wind data, and led to the selection of 9 winters out of 16 during the Odin operational period.

The ratio of NO vmr measured during the winters 2017–18 and 2018–19 to this dynamically quiet winter climatology was calculated for each altitude-time bin (1 km-1day), and the result is shown in Fig. 5 for the latitude band 70°N-90°N. This ratio is hereafter referred to as the NO excess. In 2017–18, it was oscillating around 1 (average excess = 1.02 ± 0.59, calculated over the whole altitude range), which corresponds approximately to the range of variability observed during dynamically quiet winters ([0.68;1.62]). This natural variability in middle atmospheric NO abundance is due to variations in energetic particle fluxes (auroral electrons, MEE, protons) and in solar irradiance, as well as to dynamical fluctuations (see Section 1). The NO excess was particularly low (lower than 1 at all altitudes) shortly before and after the central date in February 2018. Apart from that, similar values were observed throughout the whole winter, with no noticeable difference in the months following the SSW event. A deficit of NO was also observed around the central date in 2018–19. However, in that case, the NO excess started to significantly increase one to two weeks after the onset of the SSW event in the mid and upper mesosphere. This important excess propagated downward with time, reaching particularly high values three to five weeks after the central date in the stratopause region, where NO vmrs more the 50 times higher than the climatological values were observed. The particularly strong vertical gradient in the NO vertical distribution, as can be seen in Fig. 4, explains the increasingly high values of the NO excess at lower

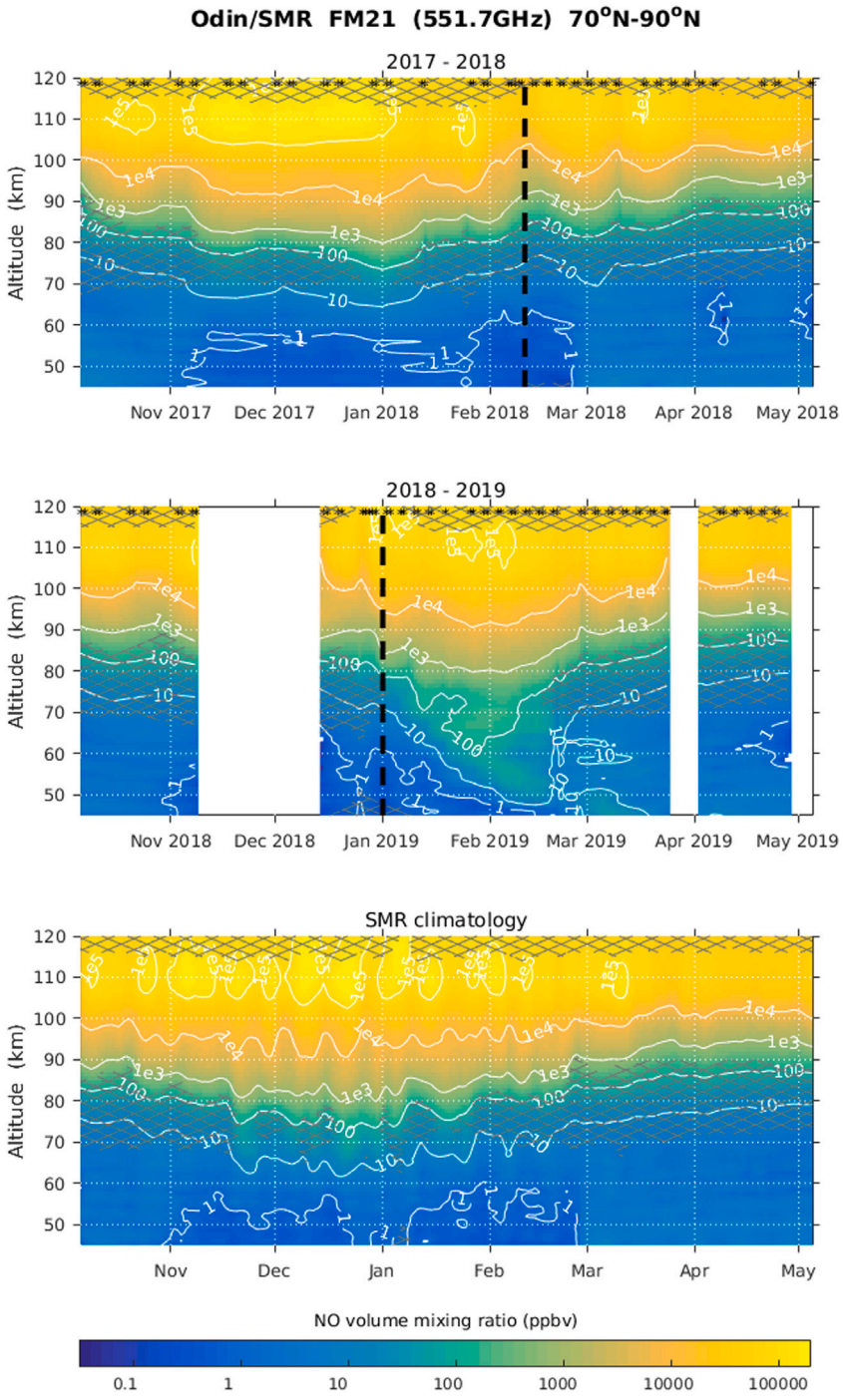

Fig. 4. Winter-time evolution of the zonal-mean NO volume mixing ratio, as observed by Odin/SMR in the latitude band [70–90]°N, as a function of altitude. The upper and middle panels correspond to the two winters under consideration, 2017–18 and 2018–19, respectively. The black vertical dashed lines indicate the central dates of the SSW events. Black stars on the top of the plots indicate the days when measurements were made. The lower panel corresponds to the SMR "quiet winter" NO climatology (see Section 4 for more details). In all panels, cross hatch patterns indicate areas with low measurement response (MR < 0.7, as defined in Section 4). White areas in the middle panel indicate the periods when no observations could be made due to instrumental problems.

altitudes where the climatological mixing ratios are low. The mean NO excess in the lower mesosphere and upper stratosphere, below 70 km, for the 80 days following the SSW central date, was 10.98, while it was very close to 1 (0.97) in 2018. Fig. 6 shows the mean NO anomalies in the altitude band 45–70 km, again at latitudes greater than 70°N, for both considered winters compared to all other winters observed by Odin with a good temporal sampling. The daily anomaly is defined here as the absolute difference between the daily mean vmr and the dynamically quiet winter climatological value (as defined hereinabove) corresponding to the same day, averaged over the indicated altitude and latitude bands. Only the data points characterised by a measurement response higher than 0.7 have been taken into account in this calculation. NO was measured during four additional northern winters, from October 2003 to April 2007, but it is not possible to follow the temporal evolution of the NO vmr in a similar way during these winters due to the low temporal sampling of the observations (see Section 2.1). For this reason, they have not been included in the figure. A strong peak in the NO anomaly appears after the event of January 2019, starting

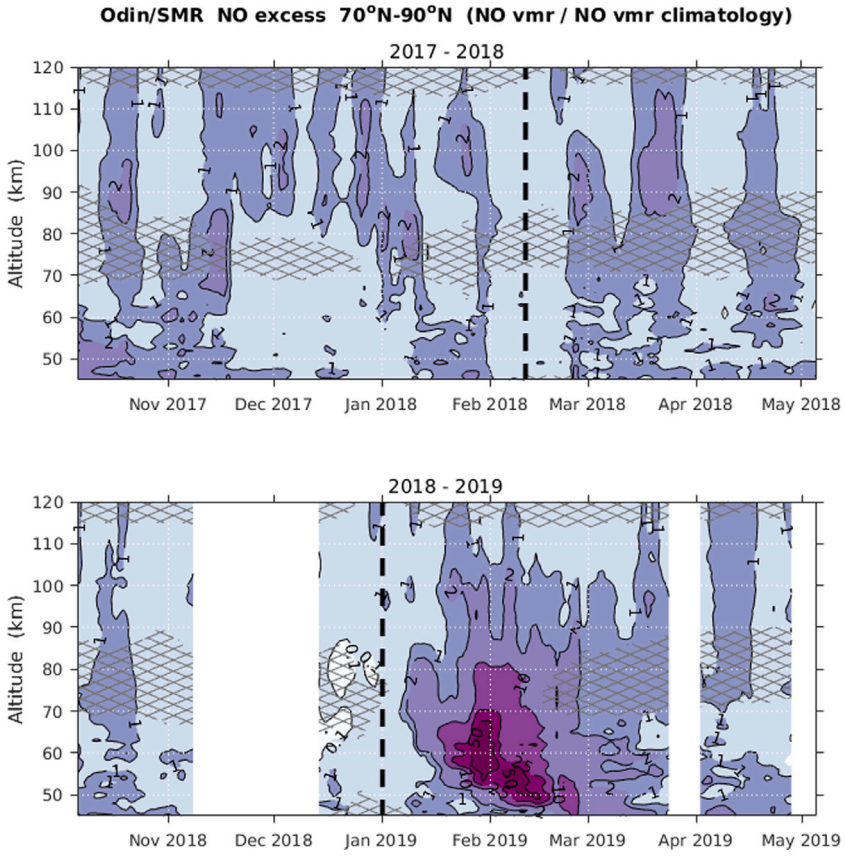

Fig. 5. Winter-time evolution of the NO excess (NO vmr/NO vmr climatology) as a function of altitude, as observed by Odin/SMR in the latitude band [70–90]°N (with contour lines corresponding to values of 0.1, 1, 2, 10, 25 and 50). The upper and lower panels correspond to the winters 2017–18 and 2018–19, respectively. Again, excess is calculated with respect to the "quiet winter" climatology. The black vertical dashed lines indicate the central dates of the SSW events and cross hatch patterns indicate areas with low measurement response (as defined in Section 4). White areas in the lower panel indicate data gaps due to instrumental problems.

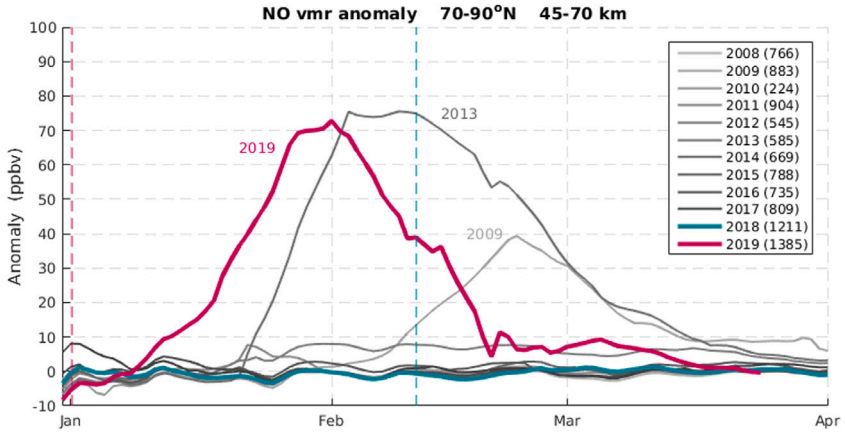

Fig. 6. Mean NO anomalies (NO vmr - NO vmr "quiet winter" climatology) in the lower mesosphere and upper stratosphere (45–70 km), at latitudes greater than 70°N, for the winters 2017–18 (green) and 2018–19 (purple), compared to all other northern winters observed by Odin/SMR after 2007 (shades of grey). The green and purple vertical dashed lines represent the central dates of the SSW events of February 2018 and January 2019, respectively. The numbers given in parentheses in the legend indicated the number of NO vertical profiles taken into account for each winter.

approximately 15 days and extending up to 80 days after the central date, reaching a maximum of 73 ppbv exactly one month after the central date. As we can see, the 2019 EPP-IE was the second strongest observed during the considered period, after the event of 2013 studied by Pérot et al. (2014) and Orsolini et al. (2017). The 2004 and 2006 SSW events, which could not be represented in this figure, also had a noticeable impact on the NO abundance in the lower mesosphere and upper stratosphere, as it can be seen in the upper panel of Fig. 3. The lower panel of this figure shows the NO vmr anomalies below 70 km (calculated in the same way as the anomalies shown in Fig. 6) averaged for the month of February, and highlights the important EPP-IE effect observed in 2006. This should however be interpreted carefully since the corresponding monthly mean value was greatly influenced by the day when the measurements were made, in this period of seldom and irregular NO observations. This histogram, combined with information on the SMR sampling times, could be a useful benchmark to test

the ability of chemistry climate models to reproduce the inter-annual variability of NO abundance at high northern latitudes. As it can be seen in both Figs. 3 and 6, the SSW event of February 2018 had on the contrary no visible effect on NO transport, with anomalies close to zero throughout the winter.

These results, based on SMR NO observations obtained during dedicated measurement campaigns, highlight the very different characteristics of the two latest winters affected by a SSW event, in term of EPP indirect effect. This will be discussed in light of the dynamical conditions in the next section.

5. Summary and conclusions

We have seen in the previous sections that, although both 2017–18 and 2018–19 winters were affected by a major SSW, the consequences these events had on the middle atmospheric NO abundance were very different. The event of February 2018 had no noticeable impact on NO, as observed by Odin/SMR. This can be explained by the fact that the SSW did not lead to a clear elevated stratopause and the zonal-mean zonal wind recovery in the mesosphere was very weak (see Fig. 2a and 2c). The conditions were not met to transport the NO down from its reservoir in the lower thermosphere towards lower altitudes, in the weeks following the central date. This winter was therefore similar to other, more dynamically quiet winters in term of EPP-IE, except around the central date, when the NO vmrs were slightly lower than the climatological values throughout the mesosphere, as seen in Fig. 5. This was due to the breakdown of the vortex, which interrupted the wintertime descent.

The EPP-IE observed after the pronounced ES-SSW of January 2019 was on the contrary one of the strongest observed during the Odin operational period. Although a slight decrease in NO mixing ratios was also observed in the days surrounding the central date, important positive anomalies were observed over the following three months in the lower mesosphere and upper stratosphere (Fig. 6), as well as values of the NO excess higher than 50 (Fig. 5). This can be explained by the dynamical perturbations at mesospheric levels, in particular the formation of a marked elevated stratopause and a strong vortex recovery (Fig. 2b and 2d) which allowed a very efficient downward transport of NO from the MLT to the lower mesosphere–upper stratosphere. We surmise that a reversal of the lower thermospheric mean meridional circulation facilitated this strong downward transport, as it was demonstrated during previous ES-SSW events (Orsolini et al., 2017). Moreover, it is noteworthy that our results are consistent with the conclusions of Holt et al. (2013). They indeed showed through model simulations that the timing of the SSW may play a significant role in determining the strength of the descent following the event, with greater descent associated with events occurring earlier in the season.

This article constitutes the first report on the impact of these two recent sudden stratospheric warmings on the middle atmospheric NO abundance in the Arctic. The study is based on measurements obtained during two dedicated observation campaigns and highlights the value of Odin/SMR, which is currently the only instrument measuring middle atmospheric NO on a global scale since other instruments in operation like SOFIE (Gómez-Ramírez et al., 2013) and ACE-FTS (Sheese et al., 2016) use solar occultations and have limited latitudinal coverage. Odin/SMR also offers the possibility to the science team to adapt the observation schedule to monitor particularly interesting atmospheric events. Here, we have chosen to focus on two specific dynamical perturbations, but we plan to develop a method to assess the amount of EPP-NO_x entering the stratosphere in both hemispheres, during the whole Odin operational period, which will allow for an optimal scientific exploitation of the SMR NO data in term of EPP-IE and will contribute to improving the representation of this effect in chemistry climate models. The global data set is available to the scientific community on the Odin/SMR website (https://odin.rss.chalmers.se/dataaccess) and allows users to investigate not only the effects of particle precipitation, but also NO variability at low and middle latitudes.

CRediT authorship contribution statement

Kristell Pérot: Conceptualisation, Planning of the observation campaigns, Methodology, Software, Interpretation of the results, Writing - original draft, Funding acquisition. **Yvan J. Orsolini:** Planning of the observation campaigns, Interpretation of the results, Writing - review & editing, Funding acquisition.

Acknowledgements

Odin is a Swedish-led satellite mission, supported by the Swedish National Space Agency (SNSA), and is also part of the European Space Agency's (ESA) third party mission programme. KP was funded by SNSA (Dnr 184/15, project "Atmospheric composition changes induced by energetic particle precipitation"). YOR was partially funded by the Research Council of Norway (grant no. 255276/E10, project SOLENA "Solar effects on natural climate variability in the North Atlantic and Arctic"). The authors would also like to thank NASA's GMAO for providing the MERRA2 data; GFZ for making the Kp-index data available; Dr Z. Lawrence for the development of the website StratObserve (https://stratobserve.com/) that was used to visualise the stratospheric forecasts and plan the special SMR observation campaigns accordingly; Stefan Lundin (OHB Sweden) and Stig Ove Silverlind (Swedish Space Corporation) for their flexibility in making quick changes in the Odin observation schedule when needed by the science team.

References

Barth, C.A., Bailey, S.M., 2004. Comparison of a thermospheric photochemical model with student nitric oxide explorer (SNOE) observations of nitric oxide. J. Geophys. Res.: Space Phys. 109 (A3), http://dx.doi.org/10.1029/2003JA010227.

Bender, S., Sinnhuber, M., von Clarmann, T., Stiller, G., Funke, B., López-Puertas, M., Urban, J., Pérot, K., Walker, K.A., Burrows, J.P., 2015. Comparison of nitric oxide measurements in the mesosphere and lower thermosphere from ACE-FTS, MIPAS, SCIAMACHY, and SMR. Atmos. Meas. Tech. 8 (10), 4171–4195. http://dx.doi.org/10.5194/amt-8-4171-2015.

Bosilovich, M.G., Akella, S., Coy, L., Cullather, R., Draper, C., Gelaro, R., Kovach, R., Liu, A.M., Norris, P., Wargan, K., Chao, W., Reichle, R., Takacs, L., Vikhliaev, Y., Bloom, S., Collow, A., Firth, S., Labow, G., Partyka, G., Pawson, S., Reale, O., Schubert, S.D., Suarez, M., 2015. MERRA-2: Initial evaluation of the climate. NASA/TM–2015-104606/Vol.43, NASA Goddard Space Flight Center.

Bosilovich, M.G., Lucchesi, R., Suarez, M., 2016. MERRA-2: File Specification No. 9 (Version 1.1). NASA Global Modeling and Assimilation Office, p. 73, https://gmao.gsfc.nasa.gov/pubs/docs/Bosilovich785.pdf.

Brasseur, G.P., Solomon, S., 2005. Aeronomy of the Middle Atmosphere, Chemistry and Physics of the Stratosphere and Mesosphere, vol. 32, Third revised and enlarged edition Springer, Dordrecht, The Netherlands.

Chandran, A., Collins, R.L., Garcia, R.R., Marsh, D.R., Harvey, V.L., Yue, J., de la Torre, L., 2013. A climatology of elevated stratopause events in the whole atmosphere community climate model. J. Geophys. Res.: Atmos. 118 (3), 1234–1246. http://dx.doi.org/10.1002/jgrd.50123.

Charlton, A.J., Polvani, L.M., 2007. A new look at stratospheric sudden warmings. Part I: Climatology and modeling benchmarks. J. Clim. 20 (3), 449–469. http://dx.doi.org/10.1175/JCLI3996.1.

Crutzen, P.J., 1970. The influence of nitrogen oxides on the atmospheric ozone content. Q. J. R. Meteorol. Soc. 96 (408), 320–325. http://dx.doi.org/10.1002/qj.49709640815.

Damiani, A., Funke, B., López Puertas, M., Santee, M.L., Cordero, R.R., Watanabe, S., 2016. Energetic particle precipitation: A major driver of the ozone budget in the antarctic upper stratosphere. Geophys. Res. Lett. 43 (7), 3554–3562. http://dx.doi.org/10.1002/2016GL068279.

Eriksson, P., 2020. Algorithm Theoretical Basis Document - Level 2 processing. Chalmers University of Technology - Department of Space, Earth and Environment, https://odin.rss.chalmers.se/static/documents/L2_ATBD.pdf.

Funke, B., Ball, W., Bender, S., Gardini, A., Harvey, V.L., Lambert, A., López-Puertas, M., Marsh, D.R., Meraner, K., Nieder, H., Päivärinta, S.-M., Pérot, K., Randall, C.E., Reddmann, T., Rozanov, E., Schmidt, H., Seppälä, A., Sinnhuber, M., Sukhodolov, T., Stiller, G.P., Tsvetkova, N.D., Verronen, P.T., Versick, S., von Clarmann, T., Walker, K.A., Yushkov, V., 2017. HEPPA-II model–measurement intercomparison project: EPP indirect effects during the dynamically perturbed NH winter 2008–2009. Atmos. Chem. Phys. 17 (5), 3573–3604. http://dx.doi.org/10.5194/acp-17-3573-2017.

Funke, B., López-Puertas, M., Stiller, G.P., von Clarmann, T., 2014. Mesospheric and stratospheric NOy produced by energetic particle precipitation during 2002–2012. J. Geophys. Res.: Atmos. 119 (7), 4429–4446. http://dx.doi.org/10.1002/2013JD021404.

Fytterer, T., Mlynczak, M.G., Nieder, H., Pérot, K., Sinnhuber, M., Stiller, G., Urban, J., 2015. Energetic particle induced intra-seasonal variability of ozone inside the antarctic polar vortex observed in satellite data. Atmos. Chem. Phys. 15 (6), 3327–3338. http://dx.doi.org/10.5194/acp-15-3327-2015, https://acp.copernicus.org/articles/15/3327/2015/.

Gelaro, R., McCarty, W., Suárez, M.J., Todling, R., Molod, A., Takacs, L., Randles, C.A., Darmenov, A., Bosilovich, M.G., Reichle, R., Wargan, K., Coy, L., Cullather, R., Draper, C., Akella, S., Buchard, V., Conaty, A., da Silva, A.M., Gu, W., Kim, G.-K., Koster, R., Lucchesi, R., Merkova, D., Nielsen, J.E., Partyka, G., Pawson, S., Putman, W., Rienecker, M., Schubert, S.D., Sienkiewicz, M., Zhao, B., 2017. The modern-era retrospective analysis for research and applications, version 2 (MERRA-2). J. Clim. 30 (14), 5419–5454. http://dx.doi.org/10.1175/JCLI-D-16-0758.1.

Global Modeling and Assimilation Office (GMAO), 2015. MERRA-2 data set tavg3_3d_asm_Nv: 3d, 3-Hourly, Time-Averaged, Model-Level, Assimilation, Assimilated Meteorological Fields V5.12.4. Goddard Earth Sciences Data and Information Services Center (GES DISC), Greenbelt, MD, USA, http://dx.doi.org/10.5067/SUOQESM06LPK, Accessed: July 2019.

Gómez-Ramírez, D., McNabb, J.W.C., Russell, J.M., Hervig, M.E., Deaver, L.E., Paxton, G., Bernath, P.F., 2013. Empirical correction of thermal responses in the solar occultation for ice experiment nitric oxide measurements and initial data validation results. Appl. Opt. 52 (13), 2950–2959. http://dx.doi.org/10.1364/AO.52.002950.

Guttu, S., Orsolini, Y., Stordal, F., Limpasuvan, V., Marsh, D.R., 2020. WACCM Simulations: Decadal winter-to-spring climate impact on middle atmosphere and troposphere from medium energy electron precipitation. J. Atmos. Sol.-Terr. Phys. 209, 105382. http://dx.doi.org/10.1016/j.jastp.2020.105382.

Hendrickx, K., Megner, L., Gumbel, J., Siskind, D.E., Orsolini, Y.J., Tyssøy, H.N., Hervig, M., 2015. Observation of 27 day solar cycles in the production and mesospheric descent of EPP-produced NO. J. Geophys. Res.: Space Phys. 120 (10), 8978–8988. http://dx.doi.org/10.1002/2015JA021441.

Holt, L.A., Randall, C.E., Peck, E.D., Marsh, D.R., Smith, A.K., Harvey, V.L., 2013. The influence of major sudden stratospheric warming and elevated stratopause events on the effects of energetic particle precipitation in WACCM. J. Geophys. Res.: Atmos. 118 (20), 11,636–11,646. http://dx.doi.org/10.1002/2013JD020294.

Karpechko, A.Y., Charlton-Perez, A., Balmaseda, M., Tyrrell, N., Vitart, F., 2018. Predicting sudden stratospheric warming 2018 and its climate impacts with a multimodel ensemble. Geophys. Res. Lett. 45 (24), 13,538–13,546. http://dx.doi.org/10.1029/2018GL081091.

Kiviranta, J., Pérot, K., Eriksson, P., Murtagh, D., 2018. An empirical model of nitric oxide in the upper mesosphere and lower thermosphere based on 12 years of odin SMR measurements. Atmos. Chem. Phys. 18 (18), 13393–13410. http://dx.doi.org/10.5194/acp-18-13393-2018.

Knight, J., Scaife, A., Bett, P.E., Collier, T., Dunstone, N., Gordon, M., Hardiman, S., Hermanson, L., Ineson, S., Kay, G., McLean, P., Pilling, C., Smith, D., Stringer, N., Thornton, H., Walker, B., 2020. Predictability of European winters 2017/2018 and 2018/2019: Contrasting influences from the tropics and stratosphere. Atmos. Sci. Lett. e1009. http://dx.doi.org/10.1002/asl.1009.

Kockarts, G., 1980. Nitric oxide cooling in the terrestrial thermosphere. Geophys. Res. Lett. 7 (2), 137–140. http://dx.doi.org/10.1029/GL007i002p00137.

Lee, S.H., Butler, A.H., 2020. The 2018–2019 arctic stratospheric polar vortex. Weather 75 (2), 52–57. http://dx.doi.org/10.1002/wea.3643.

Limpasuvan, V., Orsolini, Y.J., Chandran, A., Garcia, R.R., Smith, A.K., 2016. On the composite response of the MLT to major sudden stratospheric warming events with elevated stratopause. J. Geophys. Res.: Atmos. 121 (9), 4518–4537. http://dx.doi.org/10.1002/2015JD024401.

Lossow, S., Urban, J., Schmidt, H., Marsh, D.R., Gumbel, J., Eriksson, P., Murtagh, D., 2009. Wintertime water vapor in the polar upper mesosphere and lower thermosphere: First satellite observations by odin submillimeter radiometer. J. Geophys. Res.: Atmos. 114 (D10), http://dx.doi.org/10.1029/2008JD011462.

Lü, Z., Li, F., Orsolini, Y.J., Gao, Y., He, S., 2020. Understanding of European cold extremes, sudden stratospheric warming, and siberian snow accumulation in the winter of 2017/18. J. Clim. 33 (2), 527–545. http://dx.doi.org/10.1175/JCLI-D-18-0861.1.

Manney, G.L., Schwartz, M.J., Krüger, K., Santee, M.L., Pawson, S., Lee, J.N., Daffer, W.H., Fuller, R.A., Livesey, N.J., 2009. Aura microwave limb sounder observations of dynamics and transport during the record-breaking 2009 arctic stratospheric major warming. Geophys. Res. Lett. 36 (12), http://dx.doi.org/10.1029/2009GL038586.

Matthes, K., Funke, B., Andersson, M.E., Barnard, L., Beer, J., Charbonneau, P., Clilverd, M.A., Dudok de Wit, T., Haberreiter, M., Hendry, A., Jackman, C.H., Kretzschmar, M., Kruschke, T., Kunze, M., Langematz, U., Marsh, D.R., Maycock, A.C., Misios, S., Rodger, C.J., Scaife, A.A., Seppälä, A., Shangguan, M., Sinnhuber, M., Tourpali, K., Usoskin, I., van de Kamp, M., Verronen, P.T., Versick, S., 2017. Solar forcing for CMIP6 (v3.2). Geosci. Model Dev. 10 (6), 2247–2302. http://dx.doi.org/10.5194/gmd-10-2247-2017.

Merino, F., Murtagh, D., Ridal, M., Eriksson, P., Baron, P., Ricaud, P., Noë, J., 2002. Studies for the odin sub-millimetre radiometer: III. Performance simulations. Canad. J. Phys. 80, 357–373. http://dx.doi.org/10.1139/p01-154.

Mironova, I.A., Aplin, K.L., Arnold, F., Bazilevskaya, G.A., Harrison, R.G., Krivolutsky, A.A., Nicoll, K.A., Rozanov, E.V., Turunen, E., Usoskin, I.G.a., 2015. Energetic particle influence on the earth's atmosphere. Space Sci. Rev. 194, 1–96. http://dx.doi.org/10.1007/s11214-015-0185-4.

Mlynczak, M.G., Hunt, L.A., Marshall, B.T., Russell III, J.M., Mertens, C.J., Thompson, R.E., Gordley, L.L., 2015. A combined solar and geomagnetic index for thermospheric climate. Geophys. Res. Lett. 42 (10), 3677–3682. http://dx.doi.org/10.1002/2015GL064038.

Mlynczak, M., Martin-Torres, F.J., Russell, J., Beaumont, K., Jacobson, S., Kozyra, J., Lopez-Puertas, M., Funke, B., Mertens, C., Gordley, L., Picard, R., Winick, J., Wintersteiner, P., Paxton, L., 2003. The natural thermostat of nitric oxide emission at 5.3 μm in the thermosphere observed during the solar storms of April 2002. Geophys. Res. Lett. 30 (21), http://dx.doi.org/10.1029/2003GL017693.

Murtagh, D., Frisk, U., Merino, F., Ridal, M., Jonsson, A., Stegman, J., Witt, G., Eriksson, P., Jiménez, C., Megie, G., Noë, J.d.l., Ricaud, P., Baron, P., Pardo, J.R., Hauchecorne, A., Llewellyn, E.J., Degenstein, D.A., Gattinger, R.L., Lloyd, N.D., Evans, W.F., McDade, I.C., Haley, C.S., Sioris, C., Savigny, C.v., Solheim, B.H., McConnell, J.C., Strong, K., Richardson, E.H., Leppelmeier, G.W., Kyrölä, E., Auvinen, H., Oikarinen, L., 2002. An overview of the Odin atmospheric mission. Can. J. Phys. 80 (4), 309–319. http://dx.doi.org/10.1139/p01-157.

Orsolini, Y.J., Limpasuvan, V., Pérot, K., Espy, P., Hibbins, R., Lossow, S., Larsson, K., Murtagh, D., 2017. Modelling the descent of nitric oxide during the elevated stratopause event of January 2013. J. Atmos. Solar-Terrest. Phys. 155, 50–61. http://dx.doi.org/10.1016/j.jastp.2017.01.006.

Overland, J., Hall, R., Hanna, E., Karpechko, A., Vihma, T., Wang, M., Zhang, X., 2020. The polar vortex and extreme weather: The beast from the east in winter 2018. Atmosphere 11(6) (664), http://dx.doi.org/10.3390/atmos11060664.

Pérot, K., Urban, J., Murtagh, D.P., 2014. Unusually strong nitric oxide descent in the arctic middle atmosphere in early 2013 as observed by Odin/SMR. Atmos. Chem. Phys. 14 (15), 8009–8015. http://dx.doi.org/10.5194/acp-14-8009-2014.

Randall, C.E., Harvey, V.L., Manney, G.L., Orsolini, Y., Codrescu, M., Sioris, C., Brohede, S., Haley, C.S., Gordley, L.L., Zawodny, J.M., Russell III, J.M., 2005. Stratospheric effects of energetic particle precipitation in 2003–2004. Geophys. Res. Lett. 32 (5), http://dx.doi.org/10.1029/2004GL022003.

Randall, C.E., Harvey, V.L., Singleton, C.S., Bailey, S.M., Bernath, P.F., Codrescu, M., Nakajima, H., Russell III, J.M., 2007. Energetic particle precipitation effects on the southern hemisphere stratosphere in 1992–2005. J. Geophys. Res.: Atmos. 112 (D8), http://dx.doi.org/10.1029/2006JD007696.

Randall, C.E., Harvey, V.L., Singleton, C.S., Bernath, P.F., Boone, C.D., Kozyra, J.U., 2006. Enhanced NOx in 2006 linked to strong upper stratospheric arctic vortex. Geophys. Res. Lett. 33 (18), http://dx.doi.org/10.1029/2006GL027160.

Randall, C.E., Harvey, V.L., Siskind, D.E., France, J., Bernath, P.F., Boone, C.D., Walker, K.A., 2009. NO_X descent in the arctic middle atmosphere in early 2009. Geophys. Res. Lett. 36 (18), http://dx.doi.org/10.1029/2009GL039706.

Rao, J., Garfinkel, C.I., Chen, H., White, I.P., 2019. The 2019 new year stratospheric sudden warming and its real-time predictions in multiple S2S models. J. Geophys. Res.: Atmos. 124 (21), 11155–11174. http://dx.doi.org/10.1029/2019JD030826.

Rodgers, C.D., 2000. Inverse Methods for Atmospheric Sounding: Theory and Practice. World Scientific, http://dx.doi.org/10.1142/3171, https://www.worldscientific.com/doi/abs/10.1142/3171.

Sheese, P.E., Strong, K., Gattinger, R.L., Llewellyn, E.J., Urban, J., Boone, C.D., Smith, A.K., 2013. Odin observations of antarctic nighttime NO densities in the mesosphere–lower thermosphere and observations of a lower NO layer. J. Geophys. Res.: Atmos. 118 (13), 7414–7425. http://dx.doi.org/10.1002/jgrd.50563.

Sheese, P.E., Walker, K.A., Boone, C.D., McLinden, C.A., Bernath, P.F., Bourassa, A.E., Burrows, J.P., Degenstein, D.A., Funke, B., Fussen, D., Manney, G.L., McElroy, C.T., Murtagh, D., Randall, C.E., Raspollini, P., Rozanov, A., Russell III, J.M., Suzuki, M., Shiotani, M., Urban, J., von Clarmann, T., Zawodny, J.M., 2016. Validation of ACE-FTS version 3.5 NO_y species profiles using correlative satellite measurements. Atmos. Meas. Tech. 9 (12), 5781–5810. http://dx.doi.org/10.5194/amt-9-5781-2016.

Shepherd, M.G., Meek, C.D., Hocking, W.., Hall, C.D., Partamies, N., Sigernes, F., Manson, A.H., Ward, W.D., 2020. Multi-instrument study of the mesosphere-lower thermosphere dynamics at 80°N during the major SSW in January 2019. J. Atmos. Sol.-Terr. Phys. 210, 105427. http://dx.doi.org/10.1016/j.jastp.2020.105427.

Shi, Y., Shulga, V., Ivaniha, O., Wang, Y., Evtushevsky, O., Milinevsky, G., Klekociuk, A., Patoka, A., Han, W., Shulga, D., 2020. Comparison of major sudden stratospheric warming impacts on the mid-latitude mesosphere based on local microwave radiometer CO observations in 2018 and 2019. Remote Sens. 12 (23), http://dx.doi.org/10.3390/rs12233950.

Sinnhuber, M., Berger, U., Funke, B., Nieder, H., Reddmann, T., Stiller, G., Versick, S., von Clarmann, T., Wissing, J.M., 2018. NO_y production, ozone loss and changes in net radiative heating due to energetic particle precipitation in 2002–2010. Atmos. Chem. Phys. 18 (2), 1115–1147. http://dx.doi.org/10.5194/acp-18-1115-2018.

Sinnhuber, M., Nieder, H., Wieters, N., 2012. Energetic particle precipitation and the chemistry of the mesosphere/lower thermosphere. Surv. Geophys. 33, 1281–1334. http://dx.doi.org/10.1007/s10712-012-9201-3.

Siskind, D.E., Barth, C.A., Russell III, J.M., 1998. A climatology of nitric oxide in the mesosphere and thermosphere. Adv. Space Res. 21, 1353–1362. http://dx.doi.org/10.1016/S0273-1177(97)00743-6.

Wang, Y., Shulga, V., Milinevsky, G., Patoka, A., Evtushevsky, O., Klekociuk, A., Han, W., Grytsai, A., Shulga, D., Myshenko, V., Antyufeyev, O., 2019. Winter 2018 major sudden stratospheric warming impact on midlatitude mesosphere from microwave radiometer measurements. Atmos. Chem. Phys. 19 (15), 10303–10317. http://dx.doi.org/10.5194/acp-19-10303-2019.

Xie, J., Hu, J., Xu, H., Liu, S., He, H., 2020. Dynamic diagnosis of stratospheric sudden warming event in the boreal winter of 2018 and its possible impact on weather over north america. Atmosphere 11 (5), 438. http://dx.doi.org/10.3390/atmos11050438.